Catalysis Letters (2018) 148:3741–3749
https://doi.org/10.1007/s10562-018-2562-6

Embedding Noble-Metal-Free Ni_2P Cocatalyst on g-C_3N_4 for Enhanced Photocatalytic H_2 Evolution in Water Under Visible Light

Jianhua Ge[1,2] · **Daochuan Jiang**[1] · **Lei Zhang**[1] · **Pingwu Du**[1]

Received: 13 July 2018 / Accepted: 18 September 2018 / Published online: 8 October 2018

Abstract

Photocatalytic hydrogen evolution is considered as one of the promising pathways to settle the energy crises and environmental issues by utilizing solar energy. In this paper, noble-metal-free Ni_2P was used as cocatalyst to enhance g-C_3N_4 for photocatalytic hydrogen production under visible light irradiation ($\lambda > 420$ nm). Characterization results indicated that Ni_2P nanoparticles were successfully loaded onto g-C_3N_4, which can significantly contribute to accelerate the separation and transfer of photogenerated electron. The hydrogen evolution rate reached ~ 270 μmol h^{-1} g^{-1} and the apparent quantum yield (AQY) was ~ 2.85% at 420 nm. Meanwhile, there is no obviously decrease of the hydrogen production rate even after 36 h under visible light illumination. In addition, the mechanism of photocatalytic hydrogen evolution was also elaborated in detail.

Graphical Abstract

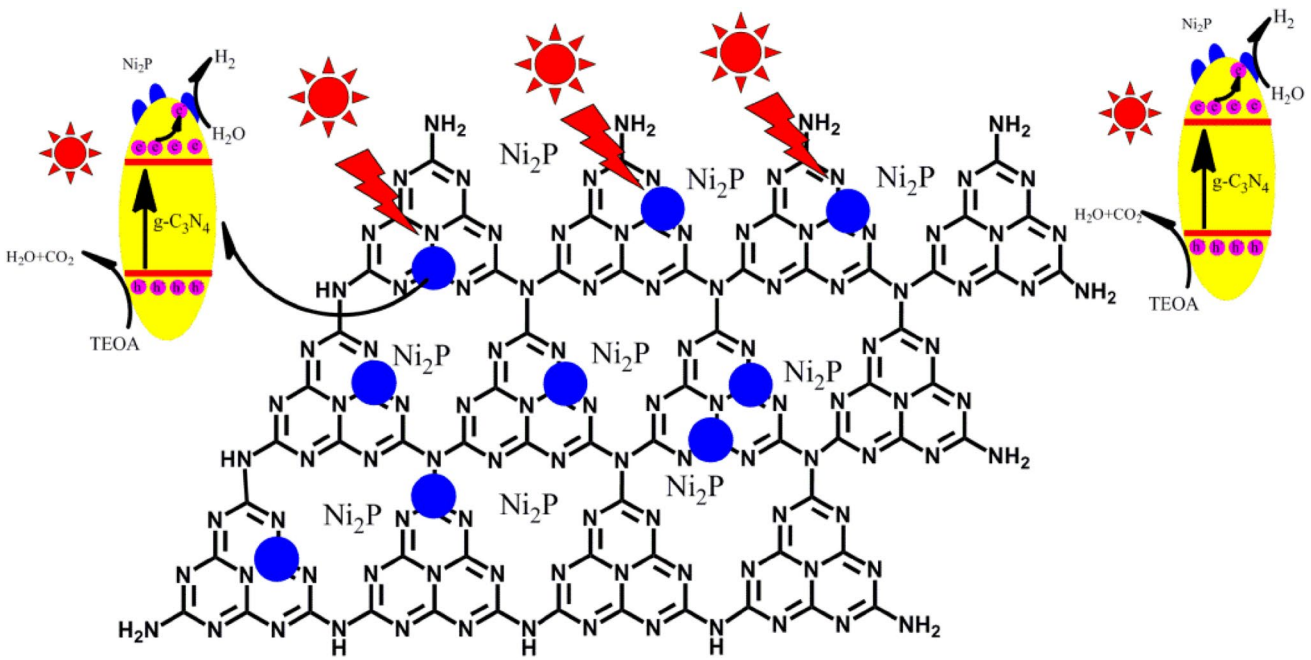

Keywords Cocatalyst · Ni_2P · Photocatalytic · Hydrogen evolution

Extended author information available on the last page of the article

1 Introduction

With aim to solve the urgent energy crisis and environmental issues in the worldwide, numerous novel and clean energy technologies were proposed [1–3]. Compared with these technologies, photocatalytic water splitting into hydrogen is widely considered as an ideal process for inexhaustible solar energy storage using semiconductors as photocatalysts [4–6]. As we all known, the photoelectrochemical cell (PEC) system for water splitting on TiO_2 photoanode under UV light has been first developed by Fujishima and Honda in 1972 [7]. Due to the obvious shortcomings of TiO_2 photocatalyst, such as wide band gap and low quantum yields [8–10]. Therefore, seeking a visible light responded photocatalyst for hydrogen generation, which possesses the characteristic of high efficiency and good stability, has become a new research hot topic in the field of solar energy conversion [11].

Very recently, a conjugated metal-free photocatalyst for hydrogen evolution, namely graphitic carbon nitride (g-C_3N_4), has drawn intensive interdisciplinary attentions owing to their moderate band gap ($E_g = 2.7$ eV), suitable band-edge positions, physicochemical stability, and fascinating electronic property and so forth [12–14]. Nevertheless, the fast recombination rate of photo-generated electron–hole pairs and low quantum efficiency restricted the photocatalytic performance of g-C_3N_4 [15, 16]. To date, a great deal of attempts has been made to enhance the photocatalytic hydrogen evolution in water of g-C_3N_4. For example surface modification [17], nano/mesoporous structures introduction [18, 19], metal element doping [15, 20], nonmetal elements doping [21], hetero-structured fabrication [22, 23], and so on. Among these strategies, loading cocatalysts on the surface of g-C_3N_4, is considered as one of the most efficient method to promote the charge separation efficiency and provides active sites for H_2 production reaction [24, 25].

More recently, development of transition metal phosphide (CoP, Ni_2P, Cu_3P, Fe_2P, MoP) to replace noble metal cocatalysts (including Pt, Au, Rh, Ru) for water splitting catalysis receives considerable attentions from researchers owing to their special metallicity and electrical conductivity [26–31]. At present, Ni_2P has been used as excellent cocatalyst for semiconductor photocatalyst. For instance our group reported that Ni_2P as a cocatalyst onto CdS NRs for photocatalytic hydrogen evolution rate reached ~ 1200 μmol h^{-1} mg^{-1} visible light, which shows extraordinarily high activity and great stability [26].

Herein, in this work, we report the noble-metal-free Ni_2P as an active cocatalyst on g-C_3N_4 semiconductors surface by in situ phosphidation method, and the hydrogen production rate has greatly improved irradiated with visible light and the AQY was ~ 2.85% at λ = 420 nm. Photoluminescence (PL) spectra and photoelectrochemical properties revealed that Ni_2P can rapidly transfer the photogenerated charge carriers of g-C_3N_4 and is a proven efficient cocatalyst for photocatalytic hydrogen production. Furthermore, the photocatalytic hydrogen evolution mechanism based on Ni_2P/g-C_3N_4 composition was proposed and also discussed in detail.

2 Experimental Details

2.1 Reagents

All the reagents (analytical grade), including sodium sulfide nonahydrate ($Na_2S{\cdot}9H_2O$, 98.0% purity), nickel nitrate hexahydrate [$Ni(NO_3)_2{\cdot}6H_2O$, 98% purity], anhydrous sodium sulfate (Na_2SO_3, 97.0% purity), urea [$CO(NH_2)_2$, 99% purity], sodium hypophosphite ($NaH_2PO_2{\cdot}H_2O$, 99% purity), and ascorbic acid ($C_6H_8O_6$, 99.7% purity), triethanolamine ($C_6H_8O_6$, 98% purity), were all purchased from Aldrich or Aladdin Reagent Co., Ltd. (China) and used without further purification.

2.2 Synthesis of the Photocatalysts

g-C_3N_4 was synthesized by a slightly modification based on a previous reports [32, 33]. In a typical procedure, 4.00 g of urea was calcined at 550 °C for 4 h in N_2 atmosphere, and the resultant product was obtained after milling.

g-C_3N_4 was decorated with different amount of Ni_2P were synthesized by annealing the mixture of $Ni(NO_3)_2{\cdot}6H_2O$, $NaH_2PO_2{\cdot}H_2O$ and g-C_3N_4 in inert atmosphere. The content of Ni_2P in the obtained samples was 0 wt%, 0.3 wt%, 0.62 wt%, 3.36 wt%, 5.98 wt% and 13.38 wt%, which were determined by ICP-AES measurements, and denoted as NC-1, NC-2, NC-3, NC-4, NC-5, and NC-6, respectively. For comparison, Ni_2P nanoparticles were also prepared using the same method in the absence of g-C_3N_4.

3 wt% Pt/g-C_3N_4 was synthesized through photodeposition process using H_2PtCl_6 as Pt source according to the previously reported literature [34].

2.3 Characterization

All the photocatalyst samples were systematically investigated by powder X-ray diffraction (XRD, D/max-TTR III, 5° min^{-1} from 10° to 70° in 2θ), Scanning electron microscope (SEM, SIRION200, equipped with an electron diffraction), Transmission electron microscopy (TEM, JEM-2010, acceleration voltage of 200 kV), High-resolution transmission electron microscopy (HR-TEM, JEM-2010, acceleration voltage of 200 kV), UV–Vis spectrometer (SOLID 3700)

and X-ray photoelectron spectroscopy (XPS, ESCALAB 250).

2.4 Photocatalytic Hydrogen Production Reactions

The photocatalytic activity reactions were performed in a 50 mL flask with magnetic stirring at room temperature using A 300 W xenon lamp as the irradiation source, which equipped with a UV cut-off filter ($\lambda > 420$ nm), and the photocatalytic hydrogen production was quantified by gas chromatography (GC, SP6890, TCD detector, high purity N_2 as a carrier gas, 5 Å molecular sieve column). For long-term photocatalytic stability under visible light irradiation, 5.0 mg of the photocatalyst sample was ultrasonic dispersed in 20 vol% TEOA aqueous solution in 250 mL flask. The apparent quantum efficiency was calculated using a 300 W Xe lamp with a band-pass filter ($\lambda = 420$ nm). A calculation of AQY was performed using following equation.

$$\text{AQY}\ (\%) = \frac{\text{Number of reacted electrons}}{\text{Number of incident photons}} \times 100\% = \frac{\text{Number of evolved } H_2 \text{ molecules} \times 2}{\text{Number of incident photons}} \times 100\%$$

3 Results and Discussion

The crystal structure of pure g-C_3N_4, pure Ni_2P and Ni_2P/g-C_3N_4 composites with different amount of Ni_2P contents (0 wt%, 0.3 wt%, 0.62 wt%, 3.36 wt%, 5.98 wt%, and 13.38 wt%) were studied by X-ray diffraction. As shown in Fig. 1, the characteristic peaks at 2θ values of 13.08° and 27.4° can be indexed to (100) and (002) crystalline planes of pure g-C_3N_4, with graphitic structure (JCPDS#87-1526) [12], and the characteristic peaks at 2θ values of peaks at 40.6°, 44.5°, 47.3°, 54.1°and 72.1°can be indexed to (111), (110), (201), (210), and (300) planes of hexagonal pure Ni_2P (JCPDS#74-1385) [35]. Meanwhile, the g-C_3N_4/Ni_2P samples with different amount of Ni_2P contents (NC-1, NC-2, NC-3, NC-4 and NC-5) display similar XRD pattern with pure g-C_3N_4, and no obvious change can be found with the Ni_2P, probably due to its low content and strong diffraction peaks of the pure g-C_3N_4. This result also indicated that the crystal structure of pure g-C_3N_4 was not changed after modification with Ni_2P.

The morphologies and material compositions of pure g-C_3N_4 and sample NC-4 were further identified by SEM, TEM and EDX. As shown in Fig. 2a, pure g-C_3N_4 displays a typical lamellar structure, and the sample NC-4 has a structure of nanoparticles closely anchored on the surface of the g-C_3N_4 nanosheets (Fig. 2b, c). In addition, the EDX spectrums (Fig. 2d) clearly reveal the existence of Ni and P elements, suggesting that Ni_2P nanoparticles were successfully loaded onto the g-C_3N_4 surface. From the TEM image of sample NC-4 (Fig. 2e), it is found that Ni_2P nanoparticles are deposited on g-C_3N_4 surface evenly. Figure 2f shows the HR-TEM image of Ni_2P composites. The lattice fringes of 0.51 nm can be assigned to the (100) plane of hexagonal pure Ni_2P [36]. Thus, these results further show that Ni_2P nanoparticles were successfully loaded onto the g-C_3N_4 nanosheets.

The oxidation states and composition of the photocatalyst sample NC-4 were further confirmed using XPS spectrum. The survey XPS scan spectrum in Fig. 3a clearly shows the existence of Ni, P, C, O and N elements, as well as O element from the absorbed gaseous molecules. Due to the low content of Ni_2P loading, the weak XPS signals were observed for Ni 2p and P 2p, which further confirm the formation of Ni 2p in the hybrids, triazine rings (C–N=C) and the tertiary nitrogen N–$(C)_3$ groups, respectively [37]. In high resolution XPS spectrum of C 1s (Fig. 3b), two deconvolution peaks at 284.6 and 288.0 eV are observed, which are assigned to graphite C–C bonds and sp^2-hybridized carbon in N-containing aromatic ring (N–C=N), respectively. The latter is considered as the major carbon species in g-C_3N_4. For the Ni 2p region, three peaks are seen at 853.2, 856.7 and 862.5 eV (Fig. 3e), which is ascribed to $Ni^{\delta+}$ ($0 < \delta < 2$) in Ni 2p, oxidized Ni species (Ni^{2+}) and the satellite of the Ni 2p1/2 peak, respectively. In addition, the other three peaks at 869.5 eV, 874.1 eV and 879.8 eV is corresponding to $Ni^{\delta+}$ in Ni 2p, oxidized Ni species and the satellite of the Ni 2p3/2 peak, respectively. For the P 2p energy level (Fig. 3f), the peak at 129.7 eV is a mark of metal-P bonds in metalphosphides (For example, Ni_2P), while the peak at 132.9 eV can be attributed to the oxidized P species due to air contact [26].

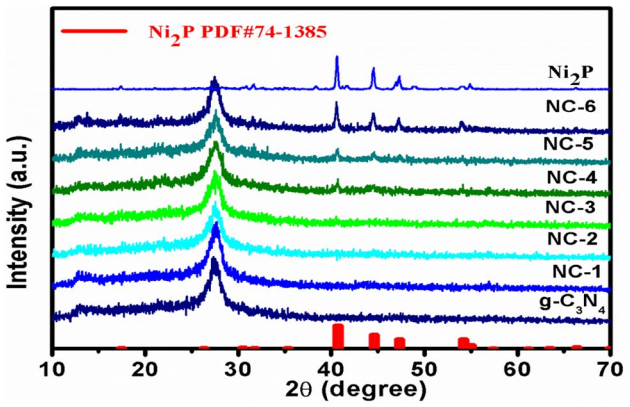

Fig. 1 XRD patterns of pure g-C_3N_4, pure Ni_2P and Ni_2P/g-C_3N_4 composites with different amount of Ni_2P contents

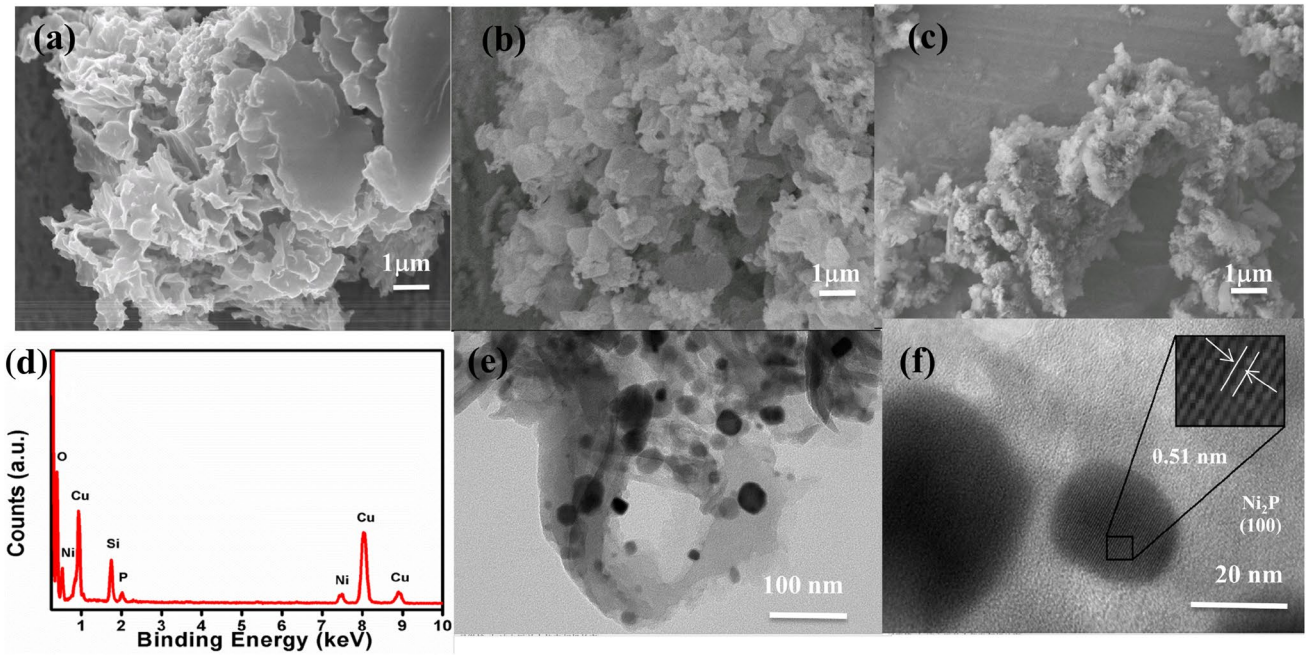

Fig. 2 The morphologies and compositions of sample: **a** SEM of g-C_3N_4, **b** SEM of NC-4, **c** SEM of Ni_2P, **d** EDX of NC-4, **e** TEM of NC-4, **f** TEM and HR-TEM of NC-4

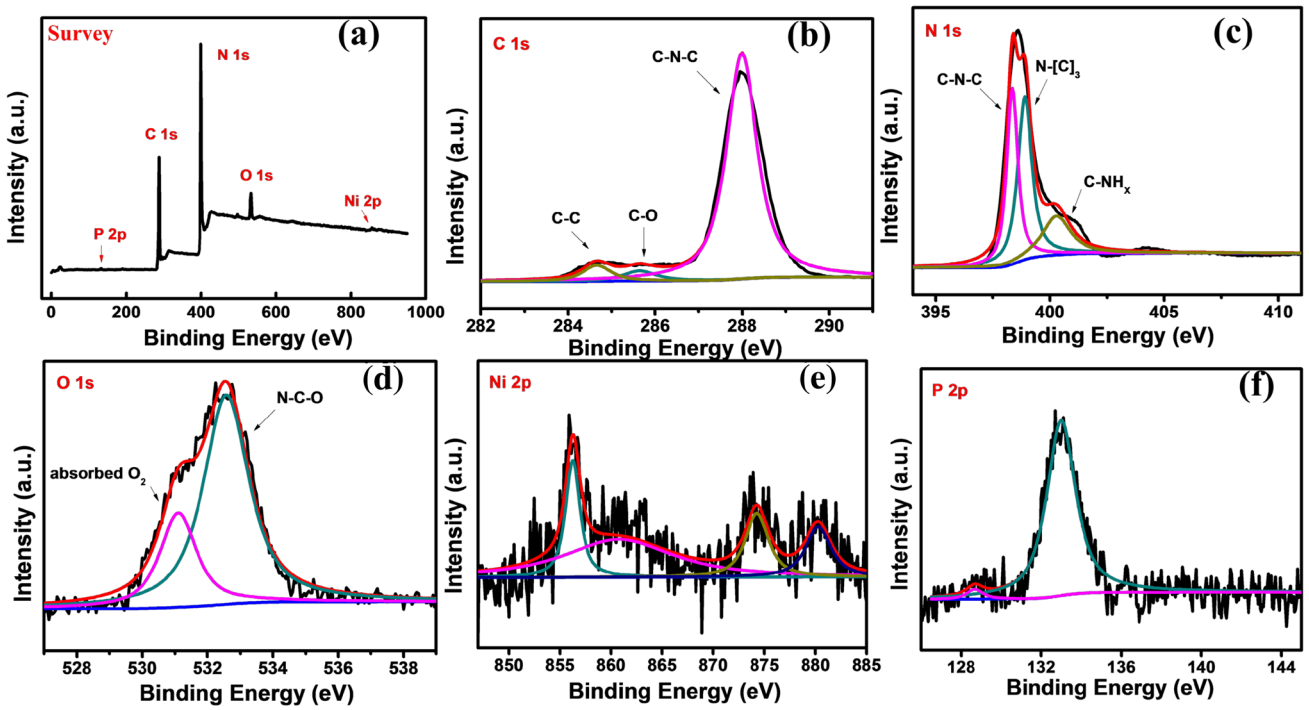

Fig. 3 XPS spectra of NC-4: **a** XPS survey, **b** C 1s peaks, **c** N 1s peaks, **d** O 1s peaks, **e** Ni 2p peaks, **f** P 2p peaks

The light harvesting properties of the pure g-C_3N_4 and NC-4 were measured by UV–Vis diffuse reflectance spectroscopy and PL spectroscopy. As depicted in Fig. 4a, the pure g-C_3N_4 sample has a sharp absorption edge at approximately 470 nm, corresponding to a band gap of ~ 2.65 eV (Fig. 4b), which is consistent with typical C materials in many previous reports [12], No obvious band-gap absorption structure throughout the UV–Vis region is

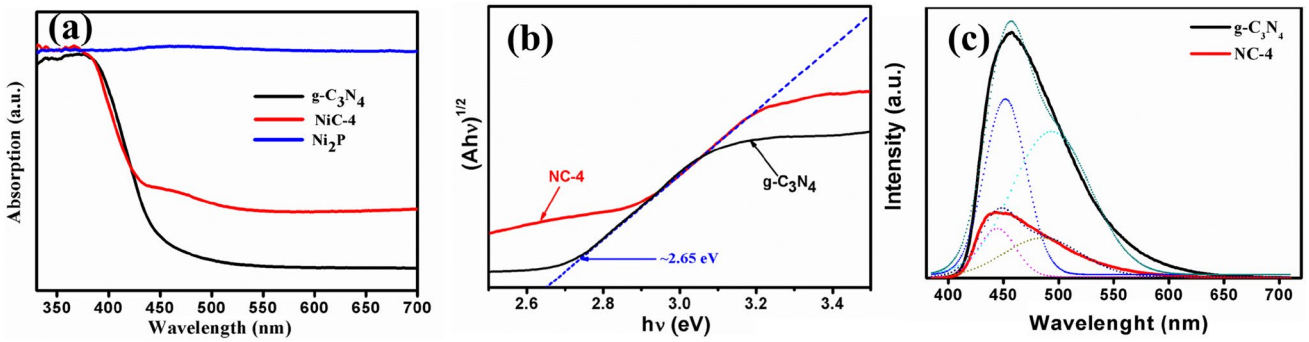

Fig. 4 UV–Vis absorption spectra and PL spectra of samples

observed for the pure Ni_2P nanoparticles, indicating a typical metallic character. As for sample NC-4, the absorption band in the region less than 470 nm is similar to that of pure g-C_3N_4 and the absorption band in the region from 470 to 700 nm is strengthened because of the presence of Ni_2P, indicating that Ni_2P was not doped into the g-C_3N_4 crystal lattice to change its band gap.

Figure 4c shows the PL spectra of pure g-C_3N_4 and sample NC-4. For pure g-C_3N_4, at an excitation wavelength of 350 nm, two distinct emission bands peaking at about 450 nm and 490 nm can be observed, which are probably due to near-band emission and surface trap state emission, respectively [38, 39]. The two peaks are remarkably quenched after loading Ni_2P onto g-C_3N_4, probably due to the fast transfer of photogenerated electrons from g-C_3N_4 to Ni_2P, indicating that the Ni_2P cocatalyst helps the transfer of charge carriers and slows down the recombination process. The photocatalytic activity for hydrogen production can be improved.

The reducing power of sample NC-4 can be evaluated by using organic electron acceptors methyl viologen dication (MV^{2+}). When the methyl viologen dication (MV^{2+}) was added to an aqueous solution containing TEOA, and 10 μg mL^{-1} sample NC-4 under visible light irradiation, the solution's color rapidly changed from light white to blue and a characteristic absorption spectrum of the methyl viologen radical cation ($MV^{+\cdot}$) appeared (Fig. 5a). This phenomenon indicated the formation of $MV^{+\cdot}$ and the fast electron transfer from the photocatalyst NC-4 to $MV^{2+\cdot}$. In addition, a diquat (DQ^{2+}, *N,N′*-(1,3-propylene)-5,5′-dimethylbipyridine dication) was also used as an electron acceptor, which has a more negative reduction potential (-0.7 V vs. NHE) than MV^{2+}. The result showed a rapid color change from light white to yellowish-brown and the appearance of the characteristic absorption spectrum of $DQ^{+\cdot}$, suggesting that the reduction potential of NC-4 is more negative than −0.7 V versus NHE, and thus the reducing power of the photoexcited electrons is sufficient for H^+ reduction to produce H_2 (Fig. 5b).

Photocatalytic hydrogen production experiments were carried out in TEOA aqueous solution. The rates of hydrogen production of pure g-C_3N_4 loaded with different

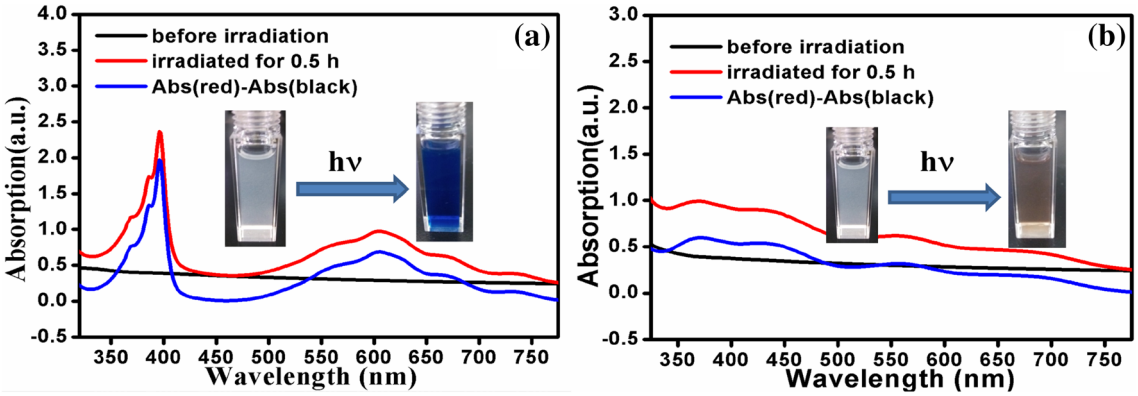

Fig. 5 Optical performance of the samples under different conditions. **a** UV–Vis absorption spectra of 3 mL aqueous solution containing TEOA, MV^{2+} (1×10^{-4} M), and sample NC-4 (10 μg mL^{-1}) before (black plot) and after visible light irradiation (red plot) for 2 min. **b** UV–Vis absorption spectra of 3 mL aqueous solution containing TEOA, DQ^{2+} (1×10^{-4} M), and sample NC-4 (10 μg mL^{-1}) before (black plot) and after visible light irradiation (red plot) for 120 s

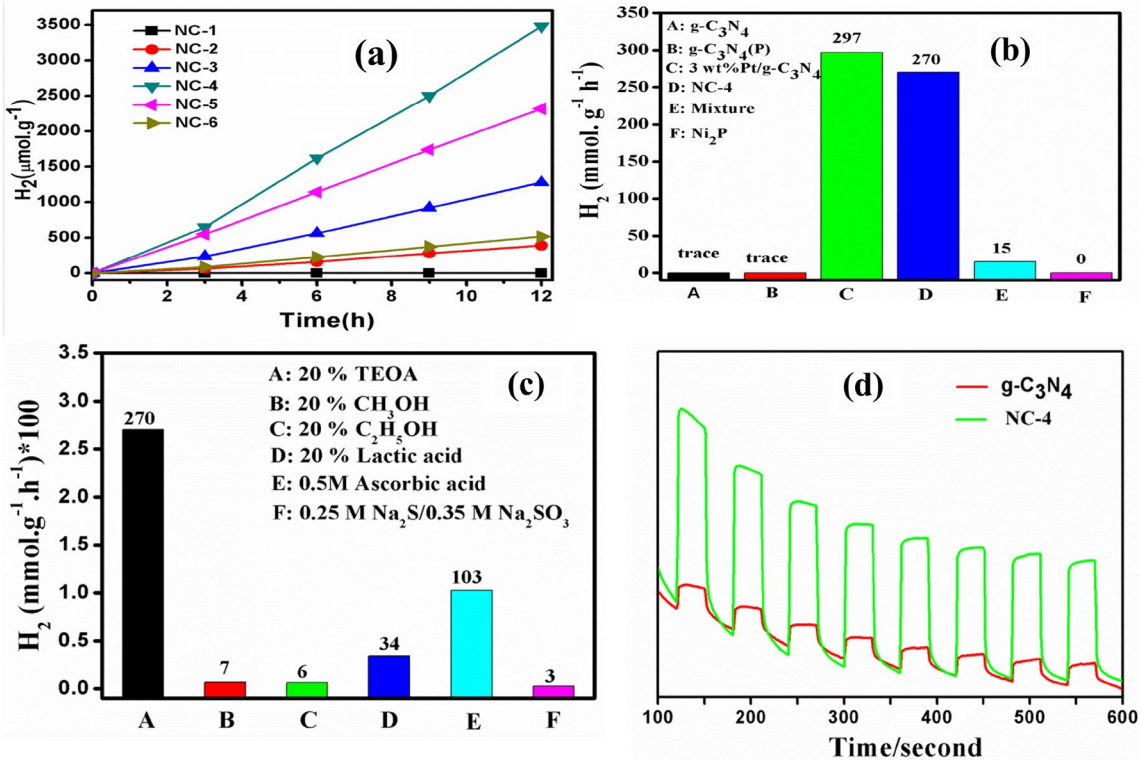

Fig. 6 Photocatalytic and photoelectrochemical activity of the samples under visible light irradiation. **a** Rates of H_2 production of $Ni_2P/g\text{-}C_3N_4$ composites. **b** Rates of H_2 production of pure $g\text{-}C_3N_4$, $Ni_2P/g\text{-}C_3N_4$ samples, pure Ni_2P and the mechanically mixed sample. **c** Rates of H_2 production of sample NC-4 in aqueous solutions with different sacrificial agent. **d** Transient photocurrent responses of pure $g\text{-}C_3N_4$ and sample NC-4 in 0.5 M Na_2SO_4 aqueous solution at 0.0 V versus Ag/AgCl

amount of Ni_2P were investigated and the results are shown in Fig. 6a. As seen in the results, the hydrogen production rate increases initially and then decreases with the increasing ratio of Ni_2P loaded, indicating that Ni_2P is an efficient cocatalyst. Nevertheless, excess Ni_2P may shield the incident light and may also block the active sites responsible for hydrogen production. Pure Ni_2P is not active for hydrogen evolution. Besides, the mechanically mixed sample of pure $g\text{-}C_3N_4$ and Ni_2P exhibits a lower rate of hydrogen production than sample NC-4, highlighting the importance of the close contact between pure $g\text{-}C_3N_4$ and the Ni_2P cocatalyst (Fig. 6b).

Photocatalytic hydrogen production experiments were further carried out using NC-4 as photocatalyst in different sacrificial electron donors (TEOA, CH_3OH, CH_3CH_2OH, Lactic acid, Ascorbic acid and concentrations of 0.75 M Na_2S and 1.05 M Na_2SO_3 aqueous solution) system. As data shows in Fig. 6c, A maximum hydrogen production rate of ~ 270 μmol h^{-1} g^{-1} can be reached in the presence of 20 vol% TEOA, which is much higher than that of pure $g\text{-}C_3N_4$, and a little lower than that of 3.0 wt% $Pt/g\text{-}C_3N_4$(~ 297 μmol h^{-1} g^{-1}). All the above results suggest that Ni_2P can effectively improve the photocatalytic activity for hydrogen production after the optimal concentration.

The transient photocurrent response curves of the electrodes coated with pure $g\text{-}C_3N_4$ and sample NC-4 were recorded for several on–off cycles. Figure 6d shows both samples present relatively low currents without light irradiation. Interestingly, an apparent increase of the photocurrent appears when visible light irradiation is turned on. When the working electrode coated with sample NC-4 exhibits a much higher photocurrent than the pure $g\text{-}C_3N_4$ electrode. The photocurrent response indicates the effective transfer of the photoinduced electrons from the photocatalyst to the back contact. Therefore, Ni_2P can efficiently facilitate the transport of photogenerated charge carriers and promote the hydrogen production activity.

Further experiments were performed to measure the AQY and confirm the long-term photocatalytic stability under visible light irradiation. Figure 7a shows that the hydrogen production rate reaches ~ 143.7 μmol^{-1} g^{-1} upon irradiation of 420 nm monochromatic in 6 h, and the values for H_2 production are relatively low in the initial few hours due to the induction period. After 6 h, the AQY is maintained at an average value of ~ 2.85%. Figure 5b shows the long-term stability for photocatalytic hydrogen production. The result shows that there is no significant decrease of the hydrogen evolution rate even after 36 h of illumination. In addition,

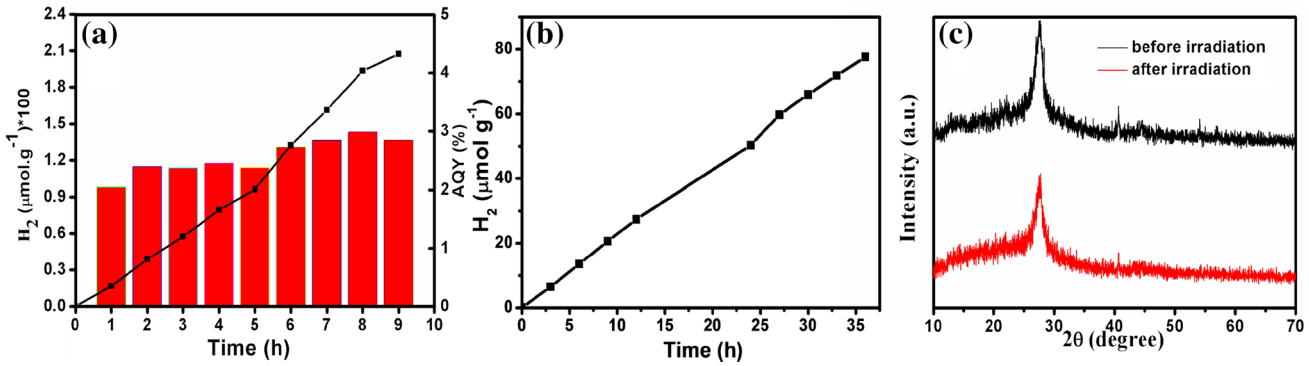

Fig. 7 Photocatalytic hydrogen production performance of sample NC-4. **a** H_2 production in different time and apparent quantum yield. **b** Long-term production of H_2 for 36 h. **c** XRD of sample NC-4 before irradiation and after irradiation

the XRD spectra of the NC-4 after irradiation show no significant difference from those before irradiation (Fig. 7c), which indicate that the Ni_2P/g-C_3N_4 photocatalyst have good photocatalytic durability and stability.

Based on the above charactertions, a possible photocatalytic mechanism of Ni_2P/g-C_3N_4 was proposed and shown in Scheme 1. When pure g-C_3N_4 is illuminated by visible light, the electrons in the valence band (VB) will be excited to the conduction band (CB). The photogenerated electrons will either recombine with the holes or transfer to the surface for photochemical hydrogen evolution reactions. As a metallic compound, Ni_2P will form a typical metal–semiconductor interface with g-C_3N_4, and the photogenerated electrons are able to transfer from the semiconductor photocatalyst g-C_3N_4 to the metallic cocatalyst Ni_2P. Thus, loading moderate Ni_2P onto g-C_3N_4 can facilitate the separation of the photogenerated electron–hole pairs in g-C_3N_4, leading to improved photocatalytic activity.

4 Conclusions

In summary, a novel Ni_2P/g-C_3N_4 photocatalyst was successfully synthesized by a facile phosphidation method. The photocatalytic activity for hydrogen production can be enhanced after the loading of Ni_2P onto g-C_3N_4. The H_2

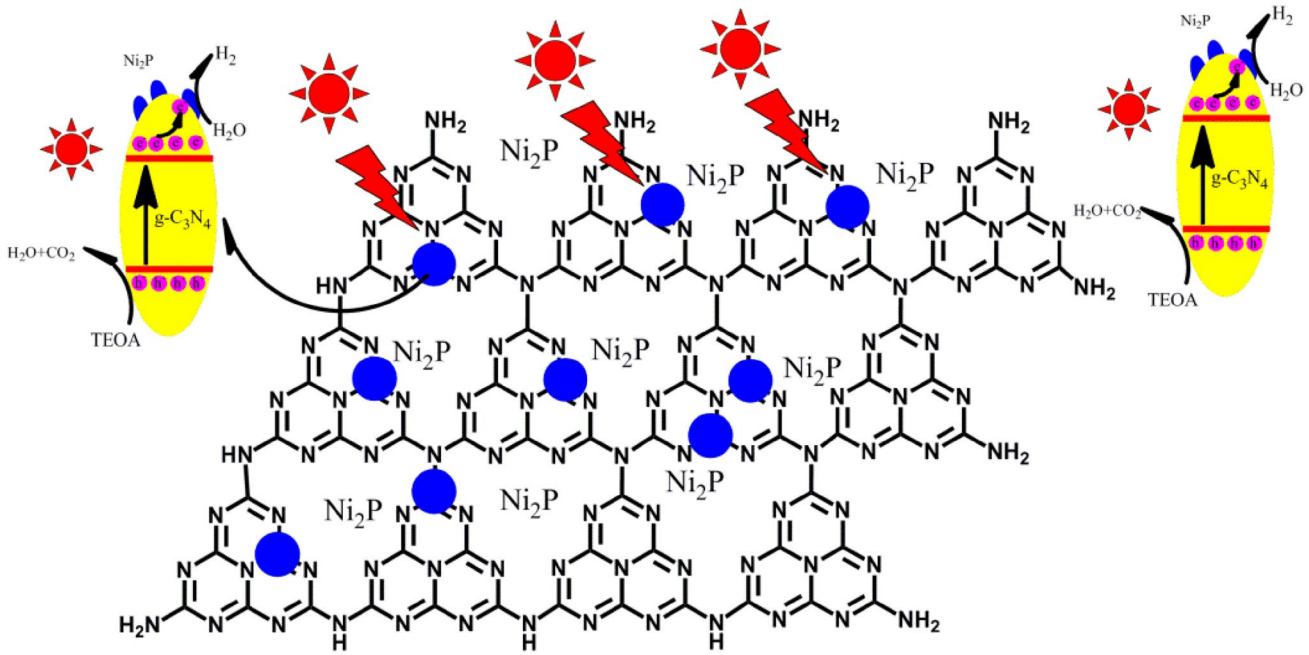

Scheme 1 Proposed mechanism for the photocatalytic hydrogen evolution over Ni_2P-loaded g-C_3N_4 semiconductor photocatalyst

production rate reached ~ 270 μmol h^{-1} g^{-1} under visible light irradiation (λ > 420 nm) and the AQY was ~ 2.85% at 420 nm. The results indicate that Ni_2P, as a noble-metal-free cocatalyst, can efficiently promote the separation of the photogenerated electron–hole pairs in g-C_3N_4. This work presents the potential of noble metal-free Ni_2P as cocatalysts for photocatalysis.

Acknowledgements This work was funded by the NSFC (21473170), the Fundamental Research Funds for the Central Universities (WK3430000001, WK2060140015, and WK2060190026), Natural science Fund of of Anhui province (1808085ME139), and The Thousand Young Talents Program.

Compliance with Ethical Standards

Conflict of interest The authors declare no competing financial interest.

References

1. Chen X, Shen S, Guo L et al (2010) Semiconductor-based photocatalytic hydrogen generation. Chem Rev 110(11):6503–6570
2. Hou Y, Wen Z, Cui S et al (2013) Constructing 2D porous graphitic C_3N_4 nanosheets/nitrogen-doped graphene/layered MoS_2 ternary nanojunction with enhanced photoelectrochemical activity. Adv Mater 25(43):6291–6297
3. Cheng J, Wang C, Cui Y et al (2014) Large improvement of visible-light-driven photocatalytic property in AgCl nanoparticles modified black BiOCl microsphere. Mater Lett 127:28–31
4. Walter MG, Warren EL, McKone JR et al (2010) Solar water splitting cells. Chem Rev 110(11):6446–6473
5. Yin Y, Guo X, Peng D (2018) Iron and manganese oxides modified maize straw to remove tylosin from aqueous solutions. Chemosphere 205:156–165
6. Dong H, Guo X, Yang C et al (2018) Synthesis of g-C_3N_4 by different precursors under burning explosion effect and its photocatalytic degradation for tylosin. Appl Catal B 230:65–76
7. Fujishima A, Honda K (1972) Electrochemical photolysis of water at a semiconductor electrode. Nature 238:37–38
8. Zhao Y, Jia X, Chen G et al (2016) Ultrafine NiO nanosheets stabilized by TiO_2 from monolayer NiTi-LDH precursors: an active water oxidation electrocatalyst. J Am Chem Soc 138(20):6517–6524
9. Zhang J, Hu Y, Jiang X et al (2014) Design of a direct Z-scheme photocatalyst: preparation and characterization of Bi_2O_3/g-C_3N_4 with high visible light activity. J Hazard Mater 280:713–722
10. Ye L, Deng K, Xu F et al (2012) Increasing visible-light absorption for photocatalysis with black BiOCl. Phys Chem Chem Phys 14(1):82–85
11. Zhou P, Yu JG, Jaroniec M. All-Solid-State (2014) Z-scheme photocatalytic systems. Adv Mater 26(29):4920–4935
12. Wang X, Maeda K, Thomas A et al (2009) A metal-free polymeric photocatalyst for hydrogen production from water under visible light. Nat Mater 8(1):76–80
13. Ong WJ, Tan LL, Ng YH et al (2016) Graphitic carbon nitride (g-C_3N_4)-based photocatalysts for artificial photosynthesis and environmental remediation: are we a step closer to achieving sustainability? Chem Rev 116(12):7159–7329
14. Chen BC, Shen Y, Wei JH et al (2016) Research progress on g-C_3N_4-based Z-scheme photocatalytic system. Acta Phys Chim Sin 32(6):1371–1382
15. Xue J, Ma S, Zhou Y et al (2015) Facile photochemical synthesis of Au/Pt/g-C_3N_4 with plasmon-enhanced photocatalytic activity for antibiotic degradation. ACS Appl Mater Interfaces 7(18):9630–9637
16. Yang XF, Chen ZP, Xu JS et al (2015) Tuning the morphology of g-C_3N_4 for improvement of Z-scheme photocatalytic water oxidation. ACS Appl Mater Interfaces 7(28):15285–15293
17. Yang LQ, Huang JF, Shi L et al (2017) A surface modification resultant thermally oxidized porous g-C_3N_4 with enhanced photocatalytic hydrogen production. Appl Catal B 204:335–345
18. Liang Q, Li Z, Huang ZH et al (2015) Holey graphitic carbon nitride nanosheets with carbon vacancies for highly improved photocatalytic hydrogen production. Adv Funct Mater 25(44):6885–6892
19. Su F, Mathew SC, Lipner G et al (2010) mpg-C_3N_4-catalyzed selective oxidation of alcohols using O_2 and visible light. J Am Chem Soc 132(46):16299–16301
20. Jiang R, Li B, Fang C et al (2014) Metal/semiconductor hybrid nanostructures for plasmon-enhanced applications. Adv Mater 26(31):5274–5309
21. Liu J, Xu H, Xu Y et al (2017) Graphene quantum dots modified mesoporous graphite carbon nitride with significant enhancement of photocatalytic activity. Appl Catal B 207:429–437
22. Cheng F, Wang H, Dong X (2015) The amphoteric properties of g-C_3N_4 nanosheets and fabrication of their relevant heterostructure photocatalysts by an electrostatic re-assembly route. Chem Commun 51(33):7176–7179
23. Di J, Xia J, Yin S et al (2014) Preparation of sphere-like g-C_3N_4/BiOI photocatalysts via a reactable ionic liquid for visible-light-driven photocatalytic degradation of pollutants. J Mater Chem A 2(15):5340–5351
24. Bai S, Yin WJ, Wang LL et al (2016) Surface and interface design in cocatalysts for photocatalytic water splitting and CO_2 reduction. RSC Adv 6(62):7446–7463
25. Ma S, Deng Y, Xie J et al (2018) Noble-metal-free Ni3C cocatalysts decorated CdS nanosheets for high-efficiency visible-light-driven photocatalytic H_2 evolution. Appl Catal B 227:218–228
26. Sun Z, Zheng H, Li J et al (2015) Extraordinarily efficient photocatalytic hydrogen evolution in water using semiconductor nanorods integrated with crystalline Ni2P cocatalysts. Energy Environ Sci 8(9):2668–2676
27. Sun Z, Yue Q, Li J et al (2015) Copper phosphide modified cadmium sulfide nanorods as a novel p-n heterojunction for highly efficient visible-light-driven hydrogen production in water. J Mater Chem A 3(19):10243–10247
28. Sun Z, Lv B, Li J et al (2016) Core-shell amorphous cobalt phosphide/cadmium sulfide semiconductor nanorods for exceptional photocatalytic hydrogen production under visible light. J Mater Chem A 4(5):1598–1602
29. Yue Q, Wan Y, Sun Z et al (2015) MoP is a novel, noble-metal-free cocatalyst for enhanced photocatalytic hydrogen production from water under visible light. J Mater Chem A 3(33):16941–16947
30. Sun Z, Chen H, Huang Q et al (2015) Enhanced photocatalytic hydrogen production in water under visible light using noble metal-free ferrous phosphide as an active cocatalyst. Catal Sci Technol 5(11):4964–4967
31. Du P, Eisenberg R (2012) Catalysts made of earth-abundant elements (Co, Ni, Fe) for water splitting: recent progress and future challenges. Energy Environ Sci 5(3):6012–6021
32. She X, Wu J, Xu H et al (2017) High efficiency photocatalytic water splitting using 2D α-Fe_2O_3/g-C_3N_4 Z-scheme catalysts. Adv Energy Mater 7(17):1700025

33. Che W, Cheng W, Yao T et al (2017) Fast photoelectron transfer in (cring)-C_3N_4 plane heterostructural nanosheets for overall water splitting. J Am Chem Soc 139(8):3021–3026
34. Xu J, Wang ZP, Zhu YF (2017) Enhanced visible-light-driven photocatalytic disinfection performance and organic pollutant degradation activity of porous g-C_3N_4 nanosheets. ACS Appl Mater Interfaces 9(33):27727–27735
35. Lin Y, Pan Y, Zhang J (2017) In-situ grown of Ni_2P nanoparticles on 2D black phosphorus as a novel hybrid catalyst for hydrogen evolution. Int J Hydrogen Energy 42(12):7951–7956
36. Wang X, Kolen'ko YV, Liu L (2015) Direct solvothermal phosphorization of nickel foam to fabricate integrated Ni_2P-nanorods/Ni electrodes for efficient electrocatalytic hydrogen evolution. Chem Commun 51(31):6738–6741
37. Ye P, Liu X, Iocozzia J et al (2017) A highly stable non-noble metal Ni_2P co-catalyst for increased H_2 generation by g-C3N4 under visible light irradiation. J Mater Chem A 5(18):8493–8498
38. Xiao J, Xie Y, Nawaz F et al (2016) Dramatic coupling of visible light with ozone on honeycomb-like porous g-C_3N_4 towards superior oxidation of water pollutants. Appl Catal B 183(Supplement C):417–425
39. Lin L, Ou H, Zhang Y et al (2016) Tri-s-triazine-based crystalline graphitic carbon nitrides for highly efficient hydrogen evolution photocatalysis. ACS Catal 6(6):3921–3931

Affiliations

Jianhua Ge[1,2] · Daochuan Jiang[1] · Lei Zhang[1] · Pingwu Du[1]

✉ Jianhua Ge
gejianhua13@163.com

✉ Pingwu Du
dupingwu@ustc.edu.cn

[1] CAS Key Laboratory of Materials for Energy Conversion, Department of Materials Science and Engineering, Collaborative Innovation Center of Chemistry for Energy Materials (iChEM), University of Science and Technology of China (USTC), Hefei 230026, Anhui, People's Republic of China

[2] School of Earth Science and Environmental Engineering, Anhui University of Science & Technology, Huainan 232001, Anhui, People's Republic of China